

## THERMAL BARRIER COATING DEBONDING DEFECTS DETECTION BASED ON INFRARED THERMAL WAVE TESTING TECHNOLOGY UNDER LINEAR FREQUENCY MODULATION HEAT EXCITATION

by

**Yuanlin LIU\***, **Guojin ZHAO**, **Yongzhi DU**, and **Yang ZHANG**

School of Mechanical Engineering, Heilongjiang University of Science and Technology,  
Harbin, China

Original scientific paper  
<https://doi.org/10.2298/TSCI180901230L>

*Thermal barrier coating debonding defects detection based on infrared thermal wave testing technology under linear frequency modulation heat excitation was studied. The principle the infrared thermal wave testing technology under linear frequency modulation was presented. The effects of different light source power and Chirp modulation frequency on signal-to-noise ratio were compared and analyzed. The results show that, defects can be more easily detected with the bigger power of light source, and the signal-to-noise ratio can be increased by using lower initial and termination frequencies.*

**Key words:** *infrared thermal wave, thermal barrier coating, debonding defects, linear frequency modulation heat excitation*

### Introduction

The thermal barrier coating (TBC) is one of the best high temperature protective coatings at present, with the characteristics of heat insulation, corrosion resistance, wear resistance and erosion resistance, has been widely used in power machinery, aerospace and other high temperature and high heat flow environment [1, 2]. During the service of TBC, defects such as cracking, debonding and even peeling of coatings are easy to occur, which will affect the operation safety and reliability of hot end components, and even have catastrophic consequences. Therefore, it is necessary to use non-destructive testing technology to detect and evaluate the state of TBC components [3, 4].

Infrared thermal wave non-destructive testing technology has the advantages of high reliability, non-contact, fast detection speed and wide detection range and has been widely used in aerospace, machinery, electronics, chemical industry, energy and many other fields [5, 6]. By applying thermal excitation the tested component, the internal defects in which will affect the heat flow conduction, resulting in abnormal temperature distribution on the surface of the component [7, 8]. The infrared thermal imager can be used to record the change of surface temperature field during the excitation process. By observing, recording and analyzing the thermal response of the component surface to the heat excitation, defects in various metals, non-metals and composite materials can be tested and evaluated.

In this paper, TBC debonding defects detection based on infrared thermal wave testing technology under linear frequency modulation (LFM) heat excitation was studied. Firstly,

\* Corresponding author, e-mail: [lyl2383849@126.com](mailto:lyl2383849@126.com)

the principle the infrared thermal wave testing technology under linear frequency modulation was presented. Secondly, experimental study was carried out, and the effects of different light source power and Chirp modulation frequency on signal-to-noise ratio (SNR) were compared and analyzed. Lastly, conclusions were is drawn.

### The principle of infrared thermal wave testing technology under LFM heat excitation

The LFM heat excitation is a new active infrared thermal wave non-destructive testing technology, which uses variable modulation frequencies to excite the tested components, and makes up for some shortcomings of pulse and lock-in method. The applied heat flux varies with time can be expressed:

$$q(t) = q_{SC} + q_{DC} = \frac{q_0}{2} \left\{ 1 + \sin \left[ 2\pi \left( f_0 + \frac{f_e - f_0}{2T_s} t \right) t \right] \right\}, t \in [0, T_s] \quad (1)$$

where  $q(t)$  means the surface heat flux,  $q_0$  – the surface heat flux peak,  $q_{SC}$  – the static component of surface heat flow,  $q_{DC}$  – the represents dynamic component of surface heat flow,  $f_0$  and  $f_e$  – the initial and termination frequencies of Chirp modulated signals, respectively, and  $T_s$  – the represents the scan cycle of Chirp modulated signals.

For simplicity, the Chirp modulation parameters are expressed by the initial frequency-termination and frequency-modulation periods. For example, 0.1-0.05-20 represents the initial frequency, and termination frequency and modulation periods are 0.1 Hz, 0.05 Hz, and 20 seconds, respectively.

### Experimental study

The detection system consists of excitation heat source, dimmer, data acquisition card, computer and infrared thermal imager. By setting the initial frequency, termination frequency, and modulation period in advance, the chirp modulation signal is output to the dimmer through data acquisition card, and the dimmer controls the modulation heat flow of halogen lamp according to the received signal. An infrared thermal imager A325SC produced by FLIR Company of the USA is used to collect the infrared radiation data, which has the advantages of high sensitivity, fast data transmission and high reliability.

The structure of TBC is three layers. The substrate is GH4169 nickel-based superalloy with the size of 140 mm × 100 mm × 5 mm. The middle bonding layer is NiCoCrAlY material. The top layer is YSZ ceramic, prepared by plasma spraying. The thermophysical parameters of the specimen and the size of simulated defects are shown in tab. 1 and tab. 2.

**Table 1. Thermophysical parameters of the specimen**

Materials	$\rho$ [kgm <sup>-3</sup> ]	$k$ [Wm <sup>-1</sup> °C <sup>-1</sup> ]	$c$ [Jkg <sup>-1</sup> °C <sup>-1</sup> ]	$\delta$ [mm]
GH4169	8300	9.5	440	5
YSZ (ZrO <sub>2</sub> + 8% wt. Y <sub>2</sub> O <sub>3</sub> )	6037	1.5	500	L
NiCoCrAlY	7320	4.3	450	0.1

The noise in infrared detection mainly comes from the background radiation of objects and atmosphere in the surrounding environment and the inherent noise of the detection system itself. Therefore, a frame of background thermal image is collected before the experiment, and then the original data of the experiment is subtracted from the collected background frame, which will lead to better experimental results. Figure 1 shows a frame of the original im-

**Table 2. Size of simulated defects**

Row	1	2	3	4	5	6
Line						
1	DA = 10.0 DL = 0.3	DA = 10.0 DL = 0.3	DA = 8.0 DL = 0.3	DA = 6.0 DL = 0.3	DA = 4.0 DL = 0.3	DA = 2.0 DL = 0.3
2	DA = 10.0 DL = 0.3	DA = 10.0 DL = 0.3	DA = 8.0 DL = 0.3	DA = 6.0 DL = 0.3	DA = 4.0 DL = 0.3	DA = 2.0 DL = 0.3
3	DA = 10.0 DL = 0.3	DA = 10.0 DL = 0.3	DA = 8.0 DL = 0.3	DA = 6.0 DL = 0.3	DA = 4.0 DL = 0.3	DA = 2.0 DL = 0.3
4	DA = 10.0 DL = 0.3	DA = 10.0 DL = 0.3	DA = 8.0 DL = 0.3	DA = 6.0 DL = 0.3	DA = 4.0 DL = 0.3	DA = 2.0 DL = 0.3

ages with modulation parameters of 0.2-0.05-20, light source power of 1400 W, sampling frequency of 30 Hz and sampling time of 20 seconds. From fig. 1, it can be seen that although some defects can be identified from the original image, the edges of defects are blurred and the noise in the defect-free area is seriously affected.

Figure 2 shows the background image collected before the experiment, from which it can be seen that the infrared radiation of the whole sample surface is not uniform due to the influence of surrounding environment and noise. The image after background subtraction is shown in fig. 3. From fig. 3, it can be seen that the contrast between defective and defective areas is significantly improved, and the edges of the defect areas is smoother and the geometric features are more obvious. Also, the original blurred and non-displayed defects are easier to identify.

In order to make the test results under different parameters can be compared under the same order of magnitude, all test data are normalized by eq. (2).

$$p = \frac{p_0 - p_{\min}}{p_{\max} - p_{\min}} \quad (2)$$

where  $p$  means the normalized test data,  $p_0$  – the raw test data,  $p_{\min}$  – the minimum value of the test data, and  $p_{\max}$  – the maximum value of the test data.

In order to compare the influence of test parameters on test results, SNR is defined eq. (3) in by taking the rectangular areas at the defect center and defect-free area as shown in fig. 4. And bigger SNR means smaller the influence of noise and stronger ability of defect detection.

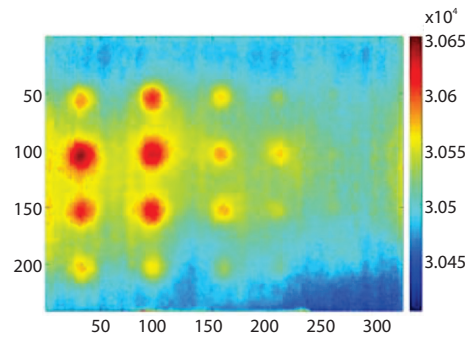


**Figure 1. A frame of the original images**

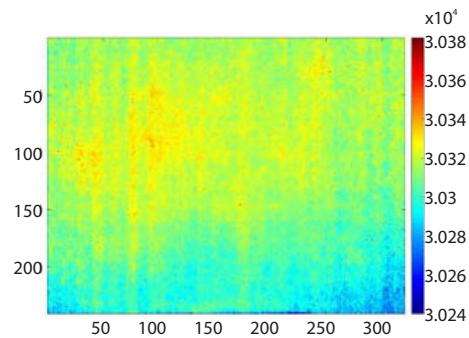


**Figure 2. The background image**

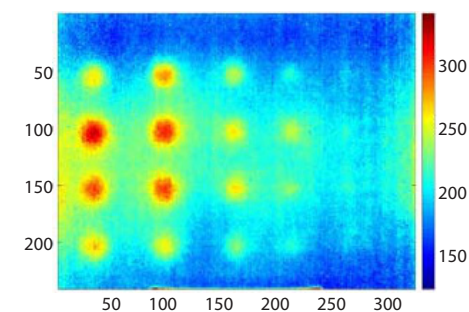


**Figure 3. The image after background subtraction**

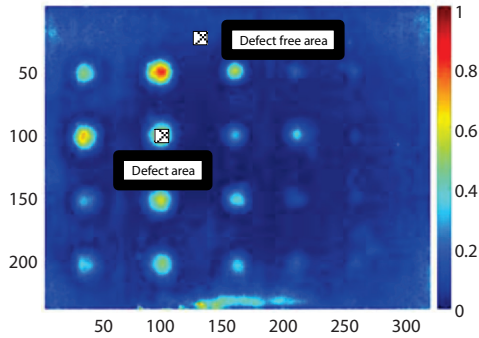


Figure 4. Reference regions for signal-to-noise ratio computation

$$\text{SNR}_d = \frac{\bar{P}_d - \bar{P}_s}{\sigma_s} \quad (3)$$

where  $\bar{P}_d$  and  $\bar{P}_s$  are the mean eigenvalue of the defective and non-defective regions, respectively,  $\sigma_s$  means the standard deviation of eigenvalues for non-defective regions, and  $\text{SNR}_d$  represents the signal-to-noise ratio of the defective regions.

## Results and discussion

### The influence of light source output power

Set Chirp modulation parameters 0.1-0.05-20, sampling time 20 seconds, sampling frequency 30 Hz, and light source output power 900 W, 1000 W, 1200 W, and 1400 W, respectively. Figure 5 shows the image with the biggest SNR corresponding to the four light source output powers. When the output power of the light source is 900 W, it is easy to identify defects in the first four columns, but the noise in non-defective areas is relatively large. When the power increases to 1000 W, the noise decreases to a certain extent. When the output power of the light source is increased to 1200 W, defects in the fifth column is more clearly displayed, and the SNR is more than 20. When the output power of the light source is increased to 1400 W, the defective regions become more obvious.

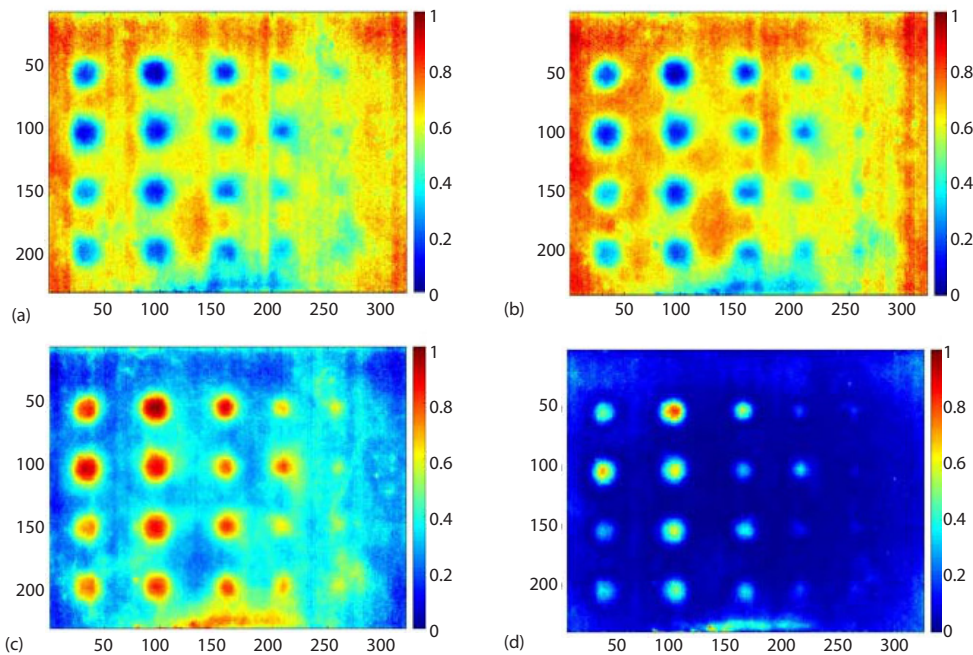


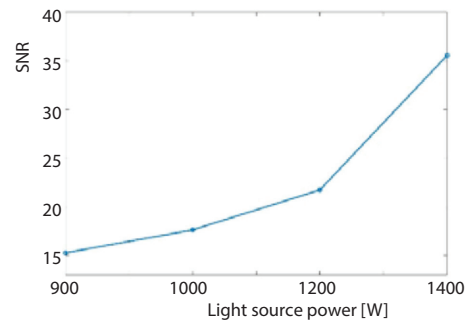
Figure 5. The influence of light source output power; (a) 900 W, (b) 1000 W, (c) 1200 W and (d) 1400 W

Figure 6 shows the influence of light source output power on SNR. Figure 6 shows that the SNR of the image increases with the increase of the output power of the light source. This shows that, on the premise of no secondary damage to the sample, the use of a larger light

source output power is conducive to improving the detection effect of defects.

*The influence of initial frequency*

Set the test sampling frequency of 30 Hz, sampling time of 20 seconds, light source output power of 1400 W, termination frequency of 0.05 Hz, modulation period of 20 seconds, and initial frequency of 0.1 Hz, 0.2 Hz, 0.3 Hz, and 0.4 Hz, respectively. Figures 7 and 8 show the influence of initial frequency on detection results. As shown in figs. 7 and 8, SNR of the image decreases with the increase of the initial frequen-



**Figure 6. The influence of light source output power on SNR**

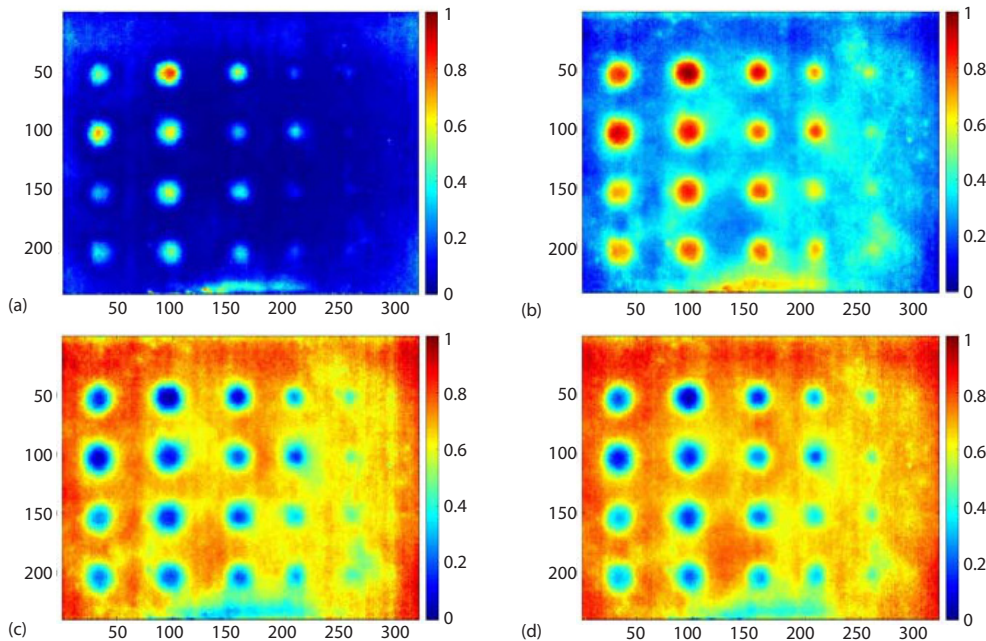


**Figure 7. The influence of initial frequency; (a) 0.1 Hz, (b) 0.2 Hz, (c) 0.3 Hz, and (d) 0.4 Hz**

cy. This shows that the lower initial frequency is helpful to improve the defect detection effect when other test parameters remain unchanged.

*The influence of termination frequency*

Set the modulation period of 20 seconds, the light source output power of 1400 W, the sampling time of 20 seconds, the sampling frequency of 30 Hz, the initial frequency of 0.45 Hz, and the termination frequency of 0.05 Hz, 0.15 Hz, 0.25 Hz, and 0.35 Hz, respectively. Figures 9 and 10 show the influence of termi-

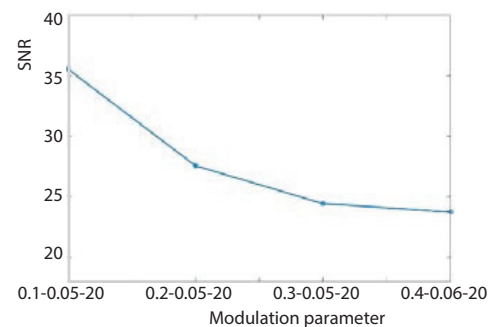


**Figure 8. The influence of initial frequency on SNR**

nation frequency on detection results. As shown in figs. 9 and 10, SNR of the image decreases with the increase of the termination frequency. This shows that the lower termination frequency is helpful to improve the defect detection effect when other test parameters remain unchanged.

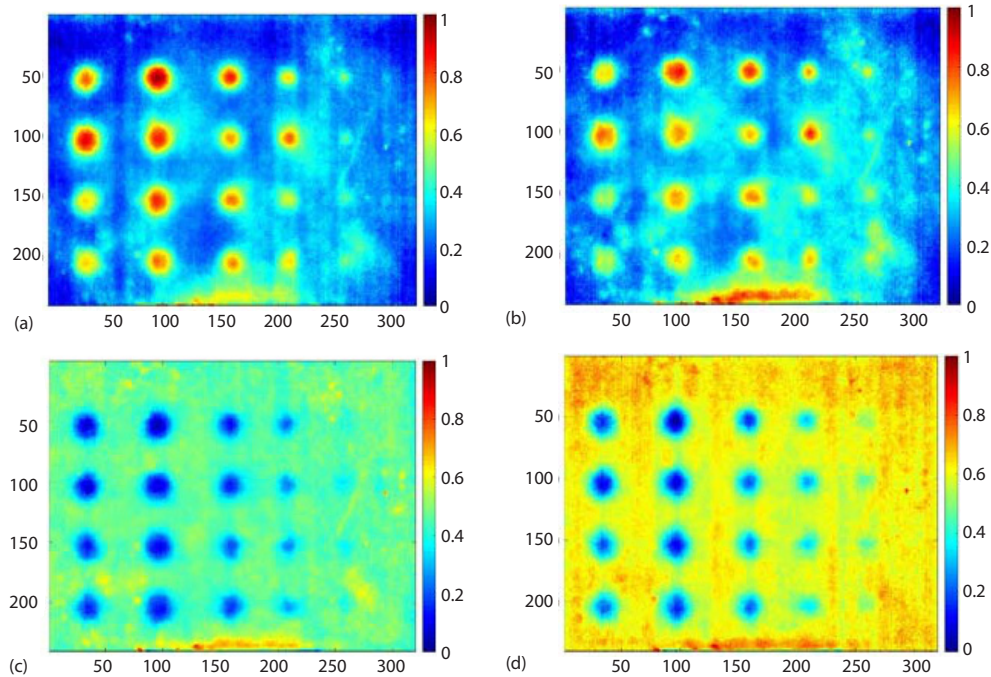


**Figure 9.** The influence of termination frequency; (a) 0.05 Hz, (b) 0.15 Hz, (c) 0.25 Hz, and (d) 0.35 Hz

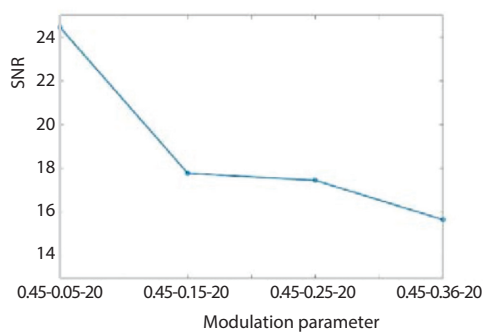


**Figure 10.** The influence of termination frequency on SNR

## Conclusions

In this study, TBC debonding defects detection based on infrared thermal wave testing technology under LFM heat excitation was studied. The principle the infrared thermal wave testing technology under linear frequency modulation was presented. Experimental study was carried out using the built up testing system, and the effects of different light source power and Chirp modulation frequency on SNR were compared and analyzed. The results show that, defects can be more easily detected with the bigger power of light source, and the SNR can be increased by using lower initial and termination frequencies. This study can provide theoretical

support for clinical application of this technology. The research can provide some basis for the actual engineering detection of debonding defects in thermal barrier coating.

## Acknowledgment

This project is supported by National Natural Science Foundation of China (Grant No. 51775175), and Science and Technology Cooperation Program of Heilongjiang Province and Chinese Academy of Sciences (Grant No. YS18A18).

## Nomenclature

$f_0$	– initial frequency, [Hz]	$q(t)$	– surface heat flux, [ $\text{Wm}^{-2}$ ]
$f_e$	– termination frequency, [Hz]	$q_{sc}$	– static component of heat flow, [ $\text{Wm}^{-2}$ ]
$q_0$	– surface heat flux peak, [ $\text{Wm}^{-2}$ ]	$T_s$	– scan cycle, [s]
$q_{DC}$	– dynamic component of surface heat flow, [ $\text{Wm}^{-2}$ ]		

## References

- [1] Gupta, M., et al., Failure Analysis of Multilayered Suspension Plasma-Sprayed Thermal Barrier Coatings for Gas Turbine Applications, *Journal of Thermal Spray Technology*, 27 (2018), 3, pp. 402-411
- [2] Jiao, D. C., et al., Exact Localization of Debonding Defects in Thermal Barrier Coatings, *AIAA Journal*, 56 (2018), 9, pp. 1-10
- [3] Fei, W., et al., Research on Debonding Defects in Thermal Barrier Coatings Structure by Thermal-Wave Radar Imaging (TWRI), *International Journal of Thermophysics*, 39 (2018), 6, pp. 71-75
- [4] Zhu, W., et al., Eddy Current Thermography with Adaptive Carrier Algorithm for Non-Destructive Testing of Debonding Defects in Thermal Barrier Coatings, *Journal of Non-Destructive Evaluation*, 37 (2018), 2, pp. 31-34
- [5] Shrestha, R., et al., Evaluation of Coating Thickness by Thermal Wave Imaging: A Comparative Study of Pulsed and Lock-in Infrared Thermography – Part I: Simulation, *Infrared Physics and Technology*, 83 (2017), 6, pp. 124-131
- [6] Murali, K., et al., Application of Image Fusion for the IR Images in Frequency Modulated Thermal Wave Imaging for Non-Destructive Testing (NDT), *Materials Today Proceedings*, 5 (2018), 1, pp. 544-549
- [7] Yang, X., General Fractional Calculus Operators Containing the Generalized Mittag-Leffler Functions Applied to Anomalous Relaxation, *Thermal Science*, 21 (2017), Suppl. 1, pp. S317-S326
- [8] Vavilov, V. P., et al., Thermal Non-Destructive Testing of Materials and Products: A Review, *Russian Journal of Non-Destructive Testing*, 53 (2017), 10, pp. 707-730